A&A 673, A34 (2023)
https://doi.org/10.1051/0004-6361/202346076

Astronomy & Astrophysics

Detection of ethanol, acetone, and propanal in TMC-1 New O-bearing complex organics in cold sources⋆

M. Agúndez[1], J.-C. Loison[2], K. M. Hickson[2], V. Wakelam[3], R. Fuentetaja[1], C. Cabezas[1], N. Marcelino[4,5], B. Tercero[4,5], P. de Vicente[5], and J. Cernicharo[1]

[1] Instituto de Física Fundamental, CSIC, Calle Serrano 123, 28006 Madrid, Spain
e-mail: marcelino.agundez@csic.es; jose.cernicharo@csic.es
[2] Institut des Sciences Moléculaires (ISM), CNRS, Univ. Bordeaux, 351 cours de la Libération, 33400 Talence, France
e-mail: jean-christophe.loison@u-bordeaux.fr
[3] Laboratoire d'Astrophysique de Bordeaux, Univ. Bordeaux, CNRS, B18N, allée Geoffroy Saint-Hilaire, 33615 Pessac, France
[4] Observatorio Astronómico Nacional, IGN, Calle Alfonso XII 3, 28014 Madrid, Spain
[5] Observatorio de Yebes, IGN, Cerro de la Palera s/n, 19141 Yebes, Guadalajara, Spain

Received 3 February 2023 / Accepted 27 March 2023

ABSTRACT

We present the detection of ethanol (C_2H_5OH), acetone (CH_3COCH_3), and propanal (C_2H_5CHO) toward the cyanopolyyne peak of TMC-1. These three O-bearing complex organic molecules are known to be present in warm interstellar clouds but had never been observed in a starless core. The addition of these three new pieces to the puzzle of complex organic molecules in cold interstellar clouds highlights the rich chemical diversity of cold dense cores in stages prior to the onset of star formation. The detections of ethanol, acetone, and propanal were made in the framework of QUIJOTE, a deep line survey of TMC-1 in the *Q* band that is being carried out with the Yebes 40 m telescope. We derive column densities of $(1.1 \pm 0.3) \times 10^{12}$ cm^{-2} for C_2H_5OH, $(1.4 \pm 0.6) \times 10^{11}$ cm^{-2} for CH_3COCH_3, and $(1.9 \pm 0.7) \times 10^{11}$ cm^{-2} for C_2H_5CHO. We investigated the formation of these three O-bearing complex organic molecules with the aid of a detailed chemical model that includes gas and ice chemistry. The calculated abundances at a time around 2×10^5 yr are in reasonable agreement with the values derived from the observations. The formation mechanisms of these molecules in our chemical model are as follows. Ethanol is formed on grains via the addition of atomic carbon on methanol followed by hydrogenation and non-thermal desorption. Acetone and propanal are produced by the gas-phase reaction between atomic oxygen and two different isomers of the C_3H_7 radical, which itself forms from the hydrogenation of C_3 on grains followed by nonthermal desorption. A gas-phase route involving the formation of $(CH_3)_2COH^+$ through several ion-neutral reactions followed by its dissociative recombination with electrons also contributes to the formation of acetone.

Key words. astrochemistry – line: identification – ISM: individual objects: TMC-1 – ISM: molecules – radio lines: ISM

1. Introduction

Interstellar clouds are known to host a wide variety of complex organic molecules (COMs). Among them are several O-bearing species with a high degree of hydrogenation, such as dimethyl ether, methyl formate, ethanol, acetone, and acetic acid, that are well known on Earth because they are used in organic chemistry laboratories. These species have traditionally been observed in warm interstellar regions, such as hot cores, hot corinos, and Galactic center clouds (Blake et al. 1987; Cazaux et al. 2003; Requena-Torres et al. 2006), where they are thought to be formed on dust grains and released to the gas phase upon thermal desorption (Garrod et al. 2008).

In recent years, O-bearing COMs typically found in warm clouds, such as methyl formate ($HCOOCH_3$) and dimethyl ether (CH_3OCH_3), have also been observed in cold clouds (Öberg et al. 2010; Cernicharo et al. 2012; Bacmann et al. 2012; Taquet et al. 2017; Jiménez-Serra et al. 2016; Soma et al. 2018; Agúndez et al. 2019, 2021). These detections came as a surprise because the mechanism responsible for the formation of these molecules in warm sources, which relies on the mobility of heavy radicals on grain surfaces and the thermal desorption of ices, is closed at the very low temperatures of these sources, typically around 10 K. Several scenarios have been proposed (e.g., Vasyunin & Herbst 2013; Ruaud et al. 2015; Balucani et al. 2015; Shingledecker et al. 2018; Jin & Garrod 2020), although there is not yet consensus on which if any is the correct one. Thus, the formation of methyl formate and dimethyl ether in cold sources continues to be an open problem in astrochemistry (Herbst & Garrod 2022).

In addition to methyl formate and dimethyl ether, two new O-bearing COMs, propenal (C_2H_3CHO) and vinyl alcohol (C_2H_3OH), were recently reported in the cold starless core TMC-1 (Agúndez et al. 2021). Here we report the detection of three new O-bearing COMs toward TMC-1: ethanol (C_2H_5OH), acetone (CH_3COCH_3), and propanal (C_2H_5CHO). These three molecules are well known in warm interstellar clouds (Snyder et al. 2002; Hollis et al. 2004; Requena-Torres et al. 2006; Lykke et al. 2017; Manigand et al. 2020) but had never before been

⋆ Based on observations carried out with the Yebes 40 m telescope (projects 19A003, 20A014, 20D023, 21A011, and 21D005). The 40 m radio telescope at Yebes Observatory is operated by the Spanish Geographic Institute (IGN; Ministerio de Transportes, Movilidad y Agenda Urbana).

observed in a cold source, at the exception of C_2H_5OH, which has been detected in L483 (Agúndez et al. 2019). We also present a detailed chemical model to investigate the formation of these O-bearing COMs in TMC-1.

2. Astronomical observations

The data presented here are part of QUIJOTE (Q-band Ultrasensitive Inspection Journey to the Obscure TMC-1 Environment; Cernicharo et al. 2021), which is an ongoing Q-band line survey carried out with the Yebes 40 m telescope at the position of the cyanopolyyne peak of TMC-1 ($\alpha_{J2000} = 4^h41^m41.9^s$ and $\delta_{J2000} = +25°41'27.0''$). Details on the line survey are given in previous papers of the QUIJOTE series (e.g., Cernicharo et al. 2021), and the adopted data reduction procedure is explained in Cernicharo et al. (2022). Briefly, QUIJOTE uses a 7 mm receiver that covers the Q band (31.0–50.3 GHz) and is connected to a fast Fourier transform spectrometer that provides a spectral resolution of 38.15 kHz (see Tercero et al. 2021). The data presented here correspond to observations carried out from November 2019 to November 2022, which amount to a total on-source telescope time of 758 h. The frequency-switching technique was used with frequency throws of 8 and 10 MHz. The intensity scale adopted is antenna temperature, T_A^*. The estimated uncertainty due to calibration in T_A^* is 10%. The antenna temperature can be converted to the main beam brightness temperature, T_{mb}, by dividing by B_{eff}/F_{eff}, where B_{eff} and F_{eff} are the beam and forward efficiencies, respectively. For the Yebes 40 m telescope in the Q band, B_{eff} can be fitted as a function of frequency as $B_{eff} = 0.797 \exp[-(\nu(\mathrm{GHz})/71.1)^2]$ using the values measured in 2022, which are reported on the web page of the Yebes 40 m telescope[1]. Measured values of F_{eff} range from 0.9 to 0.97, and here we adopt $F_{eff} = 0.97$. The half power beam width (HPBW) is given by HPBW($''$) = 1763/ν(GHz). All data were analyzed using GILDAS[2].

3. Results

3.1. Ethanol (C_2H_5OH)

Ethanol has two conformers, anti and gauche, depending on the orientation of the OH group. The most stable, and the one reported here, is the anti form, the spectroscopy of which was taken from the Cologne Database for Molecular Spectroscopy (CDMS; Müller et al. 2005)[3] and based on Pearson et al. (2008) and Müller et al. (2016). The dipole moment along the b axis (all transitions observed here are b-type) is 1.438 D (Takano et al. 1968).

We detected the four lines of anti ethanol that are predicted to be the most intense in the Q band (see Table 1 and Fig. 1). The three lines lying at 36 417 MHz, 43 026 MHz, and 46 832 MHz are detected with very high signal-to-noise ratios (S/N), $\gtrsim$15, and are precisely centered around the systemic velocity of the source, $V_{LSR} = 5.83$ km s^{-1} (Cernicharo et al. 2020). The line at 32 742 MHz is also well detected, although at a lower S/N and with an intensity lower than predicted by local thermodynamic equilibrium (LTE). For a rotational temperature of 6.0 K, as derived below for C_2H_5OH, the predicted relative intensities for the four lines, in order of increasing frequency, are 0.80:0.50:1.00:0.68. From the observed velocity-integrated intensities (see Table 1), the resulting relative intensities are 0.33:0.55:1.00:1.03. The most puzzling point is that the first line should be at least twice more intense than it is observed. We do not have a fully satisfactory explanation for this. Some weak line lying at ±8 MHz and/or ±10 MHz could be producing a negative frequency-switching artifact at the position of the 32 742 MHz line, decreasing its intensity. Alternatively, non-LTE excitation effects may be playing a role. Despite this puzzling issue of the 32 742 MHz line, we considered the detection of ethanol in TMC-1 to be secure because it would be very unlikely to have four unidentified lines that by coincidence lie at the precise frequencies of the four strongest transitions of C_2H_5OH. We note that the only previous detection of ethanol in a cold source, reported toward L483 by Agúndez et al. (2019), relied on one single line.

From a rotation diagram using the four lines of ethanol detected in TMC-1, we derive a rotational temperature (T_{rot}) of 6.0 ± 0.8 K and a column density of $(1.1 \pm 0.3) \times 10^{12}$ cm^{-2}, where we assumed a circular emission distribution with a diameter $\theta_s = 80''$ (Fossé et al. 2001). The calculated line profiles are shown in Fig. 1, where we adopt as line width the arithmetic mean of the observed Δv values.

3.2. Acetone (CH_3COCH_3)

Acetone is an asymmetric rotor in which the large-amplitude internal motion of the two equivalent methyl groups leads to level splitting into AA, EE, EA, and AE substates (Groner et al. 2002), as occurs for dimethyl ether. We adopted the spectroscopy from the Jet Propulsion Laboratory (JPL) catalogue (Pickett et al. 1998)[4]. The geometry of the molecule results in a nonzero dipole moment only along the b axis, with a measured value of 2.93 D (Peter & Dreizler 1965).

We computed the line intensities of CH_3COCH_3 in LTE adopting a rotational temperature of 6.0 K, as derived for C_2H_5OH, and focused on the ten lines predicted to be the most intense in the Q band (see Table 1 and Fig. 2). The five most intense predicted lines within this group (those with $T_{b,calc} > 1.0$ mK; see Table 1) are all detected with low to moderate S/N, in the range 5–9 σ. Among the next five lines, predicted with $T_{b,calc}$ in the range 0.6–1.0 mK (see Table 1), we only detected one line clearly, the one lying at 33 566 MHz. There is another line at 35 381 MHz predicted with a similar intensity that is detected only marginally (see Fig. 2). The three remaining lines lie above 40 GHz, where the sensitivity of the QUIJOTE data is worse than at lower frequencies. None of these three lines are clearly detected, although the observed spectra are consistent with the expected line intensities. For example, the lines at 43 604 MHz and 45 233 MHz are predicted with an intensity within the noise level of the data (see Fig. 2), while the line at 43 680 MHz is not seen because there is a negative frequency-switching artifact that lies very close to the expected position of this line (see Fig. 2). In summary, of the set of ten lines predicted to be the most intense, we detected six lines with low to moderate S/N and the four remaining lines are not detected because of insufficient sensitivity or overlap with a negative frequency-switching artifact. From our experience in the detection of molecules through weak lines with the QUIJOTE data (e.g., Agúndez et al. 2021), we consider that the detection of CH_3COCH_3 is secure because it would be very unlikely to have six lines of other species precisely centered at the frequencies of the strongest lines of acetone.

[1] https://rt40m.oan.es/rt40m_en.php
[2] http://www.iram.fr/IRAMFR/GILDAS/
[3] https://cdms.astro.uni-koeln.de/
[4] https://spec.jpl.nasa.gov/

Table 1. Observed line parameters in TMC-1.

Molecule	Transition	$\nu_{\rm calc}$ (MHz)	$E_{\rm up}$ (K)	$T_{\rm b,calc}$ [a] (mK)	$V_{\rm LSR}$ [b] (km s^{-1})	Δv [b] (km s^{-1})	$T_{\rm A}^*$ peak [b] (mK)	$\int T_{\rm A}^* {\rm d}v$ [b] (mK km s^{-1})	S/N [c] (σ)
C_2H_5OH	$4_{1,3}$–$4_{0,4}$	32 742.830	9.9	3.68	5.57 ± 0.12	1.03 ± 0.24	0.67 ± 0.17	0.73 ± 0.16	7.2
	$5_{1,4}$–$5_{0,5}$	36 417.242	14.3	2.31	5.83 ± 0.09	1.49 ± 0.22	0.76 ± 0.12	1.21 ± 0.15	14.7
	$1_{1,1}$–$0_{0,0}$	43 026.811	2.1	4.62	5.76 ± 0.04	1.09 ± 0.07	1.90 ± 0.18	2.21 ± 0.15	22.8
	$4_{0,4}$–$3_{1,3}$	46 832.826	8.4	3.14	5.68 ± 0.03	0.90 ± 0.06	2.38 ± 0.23	2.28 ± 0.15	21.1
CH_3COCH_3	$3_{0,3}$–$2_{1,2}$ *EE*	33 562.123	3.6	1.11	5.87 ± 0.14	0.99 ± 0.25	0.40 ± 0.13	0.42 ± 0.11	5.6
	$3_{0,3}$–$2_{1,2}$ *AA*	33 566.289	3.6	0.75	5.46 ± 0.10	0.90 ± 0.16	0.46 ± 0.12	0.44 ± 0.09	6.6
	$3_{1,3}$–$2_{0,2}$ *EE*	34 092.973	3.6	1.15	5.89 ± 0.17	1.36 ± 0.40	0.44 ± 0.15	0.64 ± 0.16	6.3
	$2_{2,1}$–$1_{1,0}$ *EE*	35 381.289	2.7	0.85	–	–	–	–	– [d]
	$4_{0,4}$–$3_{1,3}$ *EE*	43 597.127	5.7	1.54	5.95 ± 0.07	0.90 ± 0.16	0.79 ± 0.17	0.76 ± 0.12	9.2
	$4_{0,4}$–$3_{1,3}$ *AA*	43 604.463	5.7	0.61	–	–	–	–	– [e]
	$4_{1,4}$–$3_{0,3}$ *AE*	43 680.468	5.8	0.61	–	–	–	–	– [f]
	$4_{1,4}$–$3_{0,3}$ *EE*	43 689.327	5.7	1.54	5.73 ± 0.08	0.50 ± 0.17	0.61 ± 0.17	0.33 ± 0.10	5.4
	$4_{1,4}$–$3_{0,3}$ *AA*	43 698.504	5.7	1.03	5.84 ± 0.11	0.74 ± 0.24	0.71 ± 0.21	0.55 ± 0.16	6.0
	$3_{2,2}$–$2_{1,1}$ *EE*	45 233.560	4.6	0.94	–	–	–	–	– [e]
C_2H_5CHO	$4_{0,4}$–$3_{1,3}$	32 897.820	5.0	0.72	–	–	–	–	– [d]
	$3_{1,2}$–$2_{1,1}$	33 346.830	3.8	0.96	5.59 ± 0.15	0.99 ± 0.26	0.38 ± 0.10	0.40 ± 0.11	6.9
	$3_{1,3}$–$2_{0,2}$	39 061.035	3.4	1.10	5.78 ± 0.10	0.79 ± 0.20	0.45 ± 0.15	0.38 ± 0.09	5.3
	$4_{1,4}$–$3_{1,3}$	39 177.138	5.3	1.26	5.93 ± 0.10	0.73 ± 0.18	0.46 ± 0.15	0.36 ± 0.09	5.2
	$4_{0,4}$-$3_{0,3}$	40 915.768	5.0	1.47	5.81 ± 0.12	1.11 ± 0.31	0.59 ± 0.16	0.70 ± 0.16	7.9
	$4_{2,3}$–$3_{2,2}$	41 883.719	7.2	0.78	–	–	–	–	– [f]
	$4_{2,2}$–$3_{2,1}$	42 936.277	7.3	0.80	–	–	–	–	– [e]
	$5_{0,5}$–$4_{1,4}$	44 189.959	7.4	0.97	–	–	–	–	– [f]
	$4_{1,3}$–$3_{1,2}$	44 319.499	5.9	1.30	6.07 ± 0.07	0.56 ± 0.19	0.67 ± 0.18	0.40 ± 0.11	5.8
	$4_{1,4}$–$3_{0,3}$	47 195.073	5.3	1.31	5.90 ± 0.11	0.89 ± 0.29	0.92 ± 0.25	0.88 ± 0.22	7.6
	$5_{1,5}$–$4_{1,4}$	48 801.725	7.6	1.40	5.63 ± 0.11	0.60 ± 0.19	0.79 ± 0.28	0.51 ± 0.16	4.9

Notes. [a] $T_{\rm b,calc}$ is the peak brightness temperature calculated in local thermodynamic equilibrium for a rotational temperature of 6.0 K. We adopted the column density and line width derived for each molecule (see Sect. 3). [b] The line parameters $V_{\rm LSR}$, Δv, $T_{\rm A}^*$ peak, and $\int T_{\rm A}^* {\rm d}v$ and the associated errors are derived from a Gaussian fit to each line profile. Δv is the full width at half maximum. [c] The signal-to-noise ratio is computed as $S/N = \int T_{\rm A}^* {\rm d}v / [{\rm rms} \times \sqrt{\Delta v \times \delta v (c/\nu_{\rm calc})}]$, where c is the speed of light, δv is the spectral resolution (0.03815 MHz), the rms is given in the uncertainty of $T_{\rm A}^*$ peak, and the rest of the parameters are given in the table. [d] Line is only marginally detected. [e] Line is not detected. Expected intensity is within the noise level. [f] Line is not detected. It overlaps with a negative frequency-switching artifact.

The six detected lines cover a low range of upper level energies and their velocity-integrated intensities have non-negligible errors, which makes it difficult to precisely determine the rotational temperature of CH_3COCH_3. We therefore adopted a rotational temperature of 6.0 K, as determined for C_2H_5OH, and a source size with a diameter of 80″, as adopted for C_2H_5OH, and derived a column density of $(1.4 \pm 0.6) \times 10^{11}$ cm^{-2} for CH_3COCH_3. The calculated line profiles, adopting as line width the average of the Δv values observed, are shown in Fig. 2.

3.3. Propanal (C_2H_5CHO)

Propanal has two conformers, syn and gauche, depending on the orientation of the CHO group. The most stable one is the *syn* form, which is the one detected in TMC-1. The rotational spectroscopy was taken from the CDMS (Müller et al. 2005) and is mostly based on Zingsheim et al. (2017). The components of the dipole moment along the *a* and *b* axes are 1.71 D and 1.85 D, respectively (Butcher & Wilson 1964). Both *a*- and *b*-type transitions are observed here.

Similarly to the case of acetone, we computed the line intensities in LTE of syn propanal assuming a rotational temperature of 6.0 K and focused on the lines expected with a brightness temperature, $T_{\rm b,calc}$, above 0.7 mK. The 11 resulting lines are given in Table 1 and shown in Fig. 3. There are eight lines within this selected group that are predicted with $T_{\rm b,calc} > 0.9$ mK, from which we detected seven lines with low to moderate S/N in the range 5–8 σ. The remaining line at 44 189 MHz overlaps with a negative artifact resulting from the frequency-switching technique (see Fig. 3). The other three lines predicted to be less intense, with $T_{\rm b,calc}$ in the range 0.7–0.9 mK, are not clearly detected for different reasons. The line at 32 897 MHz is only marginally detected, the one at 41 883 MHz overlaps with a negative frequency-switching artifact, and the last one at 42 936 MHz is predicted with an intensity within the noise level of the data. Even if the lines of propanal are detected with relatively low S/N, we are confident about the detection due to the high number of detected lines (seven) and because we can explain the lines that are not detected on the basis of insufficient sensitivity of overlap with negative artifacts from the frequency-switching observing mode. As in the case of acetone, it would be very unlikely to have seven lines from different species located at the precise frequencies of the most intense lines of syn propanal.

As in the case of acetone, the sizable errors in the velocity-integrated intensities do not allow the rotational temperature of propanal to be precisely constrained. We therefore adopted a rotational temperature of 6.0 K, as determined for C_2H_5OH. As with the previous molecules, we adopted an emission distribution with a diameter of 80″. The column density derived for C_2H_5CHO is $(1.9 \pm 0.7) \times 10^{11}$ cm^{-2}. In Fig. 3, we show the line profiles computed, where we adopted as full width at half maximum (FWHM) the mean of the observed Δv values.

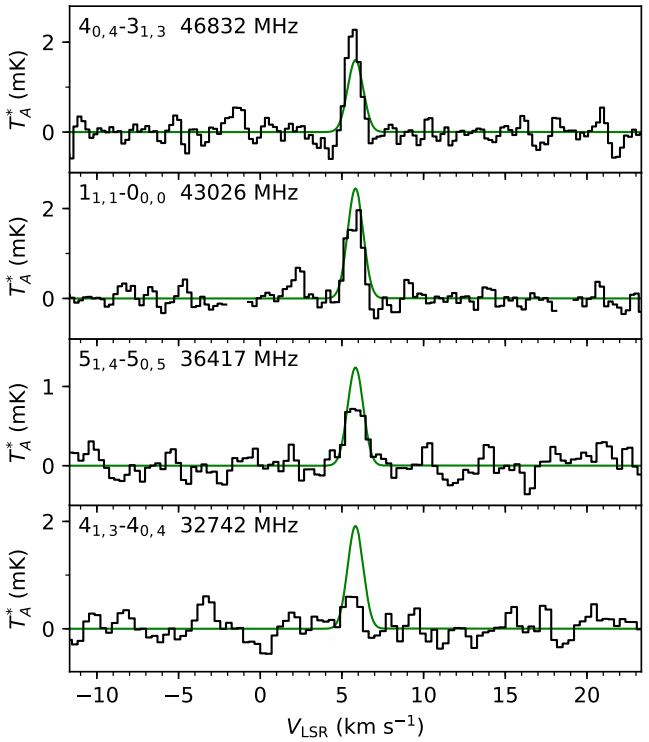

Fig. 1. Lines of C_2H_5OH observed in TMC-1 (see the parameters in Table 1). In green we show the calculated spectra for $N = 1.1 \times 10^{12}$ cm^{-2}, $T_{rot} = 6.0$ K, FWHM = 1.13 km s^{-1}, and $\theta_s = 80''$.

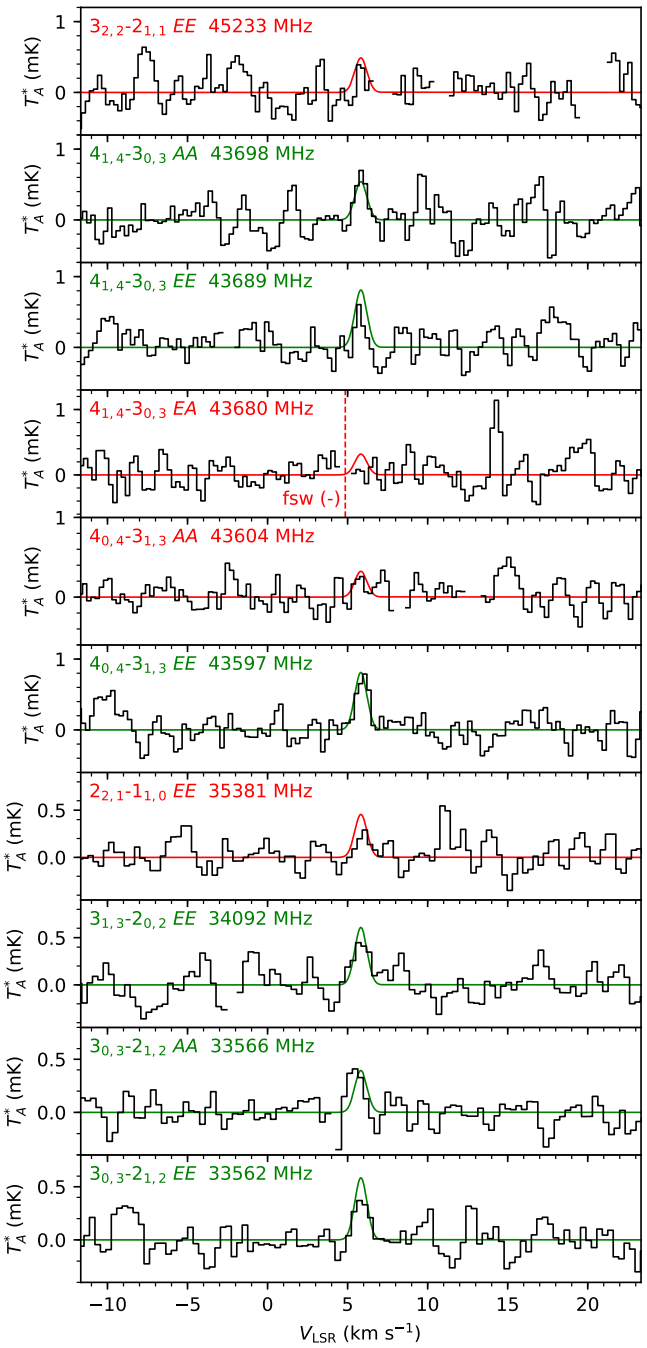

Fig. 2. Lines of CH_3COCH_3 observed in TMC-1 shown from bottom to top in order of increasing frequency (see Table 1). The panels in green show the lines that are well detected, while those in red show lines that are not clearly detected due to a variety of reasons (see the text and caption in Table 1). The position of a negative frequency-switching artifact is indicated with a dashed vertical line and labeled as "fsw (-)". The solid green and red lines correspond to the calculated spectra for $N = 1.4 \times 10^{11}$ cm^{-2}, $T_{rot} = 6.0$ K, FWHM = 0.90 km s^{-1}, and $\theta_s = 80''$.

4. Chemical model

To describe the chemistry of O-bearing COMs in TMC-1, we used the Nautilus code, which is a three-phase (gas, dust grain ice surface, and dust grain ice mantle) time-dependent chemical model (Ruaud et al. 2016). The code has recently been updated with a better description of the chemistry of COMs in the gas phase and on grains (Manigand et al. 2021; Coutens et al. 2022) and with the inclusion of sputtering of ices by cosmic rays (Wakelam et al. 2021). To describe the physical conditions in TMC-1, we used a homogeneous cloud with an H_2 volume density of 2.5×10^4 cm^{-3}, a temperature of 10 K for both gas and dust, a visual extinction of 30 mag, and a cosmic-ray ionization rate of H_2 of 1.3×10^{-17} s^{-1}. All elements are assumed to be initially in atomic form, except for hydrogen, which is entirely molecular. The initial abundances are those of Table 1 of Hincelin et al. (2011), the C/O elemental ratio being equal to 0.7 in that study.

The calculated abundances relative to H_2 for the O-bearing COMs detected in this study are shown in Fig. 4. The observed abundances are relatively well reproduced by the model for a cloud age of around 2×10^5 yr. It should be noted that although the destruction pathways of COMs are fairly well constrained, this is not the case for the formation pathways. Destruction of COMs occurs mainly through reactions with H_3^+ and atomic carbon. The reactions with H_3^+ are an important destruction pathway for COMs because not only is the protonated form usually a minor product (Lee et al. 1992), but the electronic dissociative recombination (DR) of the protonated form gives back very little of the original COM. For example, the DR of $C_2H_5OH_2^+$ produces less than 7% of C_2H_5OH (Hamberg et al. 2010). The reactions with C are also an important destruction pathway for COMs because atomic carbon seems to react with numerous COMs without a barrier (Husain & Ioannou 1999; Shannon et al. 2014; Hickson et al. 2021). The other important destruction pathways are the reactions with C^+, H^+, S^+, and He^+. With regard to the formation of O-bearing COMs in cold molecular clouds, there are several very different possible pathways.

First, bimolecular reactions between atomic oxygen and hydrocarbon radicals can be an important source of O-bearing COMs. Since atomic oxygen is highly abundant, this mechanism

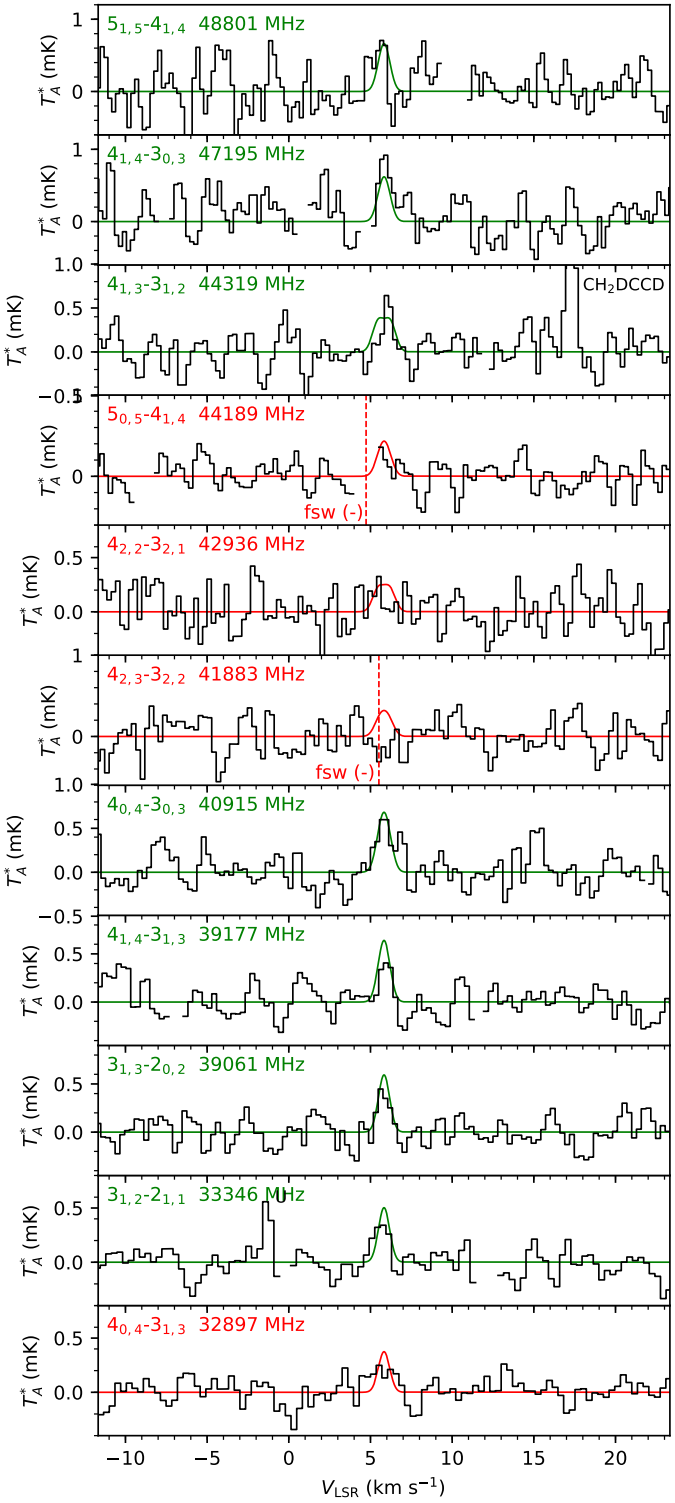

Fig. 3. Same as Fig. 2 but for C_2H_5CHO, i.e., detected lines in green and non-detected lines in red (see the line parameters in Table 1). The solid green and red lines correspond to the calculated spectra for $N = 1.9 \times 10^{11}$ cm^{-2}, $T_{rot} = 6.0$ K, FWHM = 0.81 km s^{-1}, and $\theta_s = 80''$.

can be very efficient when the hydrocarbon radical is present with a high enough abundance. Acetone is produced through the O + 2-C_3H_7 (CH_3CHCH_3) reaction, and propanal is produced through the O + 1-C_3H_7 ($CH_2CH_2CH_3$) reaction (Tsang & Hampson 1986; Hoyermann & Sievert 1979). In our present version of the model, we consider that C_3 does not react with oxygen atoms (Woon & Herbst 1996), which results in high abundances of C_3 derivatives in the ice (Hickson et al. 2016) and a notable abundance of the C_3H_7 radical in the gas phase due to chemical desorption (Garrod et al. 2007; Minissale et al. 2016) and cosmic-ray sputtering (Wakelam et al. 2021). This is the main formation pathway for C_2H_5CHO and an important one for CH_3COCH_3.

Second, radiative association between neutral radicals can directly produce O-bearing COMs. For example, the association of CH_3 and CH_2OH can yield C_2H_5OH, while CH_3 + CH_3CO can form CH_3COCH_3. These two reactions have not been studied to the best of our knowledge but are likely to be fast by comparison with CH_3 + $CH_3O \rightarrow CH_3OCH_3 + h\nu$ (Tennis et al. 2021). However, these reactions are not very efficient in our TMC-1 model because the calculated abundances of CH_2OH and CH_3CO are too small. It would be interesting to search for CH_2OH, a species whose microwave spectroscopy has recently been studied (Bermúdez et al. 2017; Chitarra et al. 2020; Coudert et al. 2022), to see if its abundance is significantly higher than calculated, which could increase the role of radiative associations between neutrals in the synthesis of COMs, as suggested by Balucani et al. (2015).

The third way to produce O-bearing COMs is the DR of their protonated form. However, there are relatively few reactions that produce the protonated form of COMs, mostly ion-neutral radiative associations, which compete with the faster proton transfer channel when this is exothermic. We used the reactions and rate coefficients from Herbst (1987) and Herbst et al. (1990) to produce C_2H_5CHO and CH_3COCH_3, reviewing the different pathways to $(CH_3)_2COH^+$, in addition to the one postulated by Herbst et al. (1990), CH_3^+ + CH_3CHO (see Appendix A). In any case, these routes play a secondary role in the formation of the O-bearing COMs observed in this study except for CH_3COCH_3, in which case the pathway initiated by the reaction OH + $C_3H_7^+$ is favored by the important production of C_3 and its derivatives.

The last possible means of COM production is through their synthesis on grains followed by desorption. As the majority of species are not mobile on grains at 10 K, except for atomic hydrogen and, to a lesser extent, atomic nitrogen, this requires an abundant precursor in the gas phase and an efficient low temperature desorption mechanism, such as chemical desorption (Garrod et al. 2007; Minissale et al. 2016) or cosmic-ray sputtering (Wakelam et al. 2021). This is the case for methanol, formed from the surface hydrogenation of CO produced in the gas phase. This is also potentially the case for C_3 derivatives (methylacetylene, propene, and propane) if C_3 does not react with atomic oxygen (Woon & Herbst 1996; Hickson et al. 2016), but it is not the case for COMs in general. However, since atomic carbon reacts without a barrier with species on grains such as H_2CO (Husain & Ioannou 1999) and CH_3OH (Shannon et al. 2014), the reactive sticking of carbon atoms to the grains induces the formation of COMs through an Eley-Rideal mechanism, as discussed by Ruaud et al. (2015). In particular, in our model C_2H_5OH is mainly formed by the insertion of the C atom into the C−O bond of CH_3OH followed by hydrogenation.

In summary, our chemical model indicates that C_2H_5OH is mostly produced on grains, C_2H_5CHO is mainly formed by the reaction O + 1-C_3H_7, where 1-C_3H_7 is itself produced on grains, and CH_3COCH_3 is produced by the O + 2-C_3H_7 reaction (2-C_3H_7 is itself produced on grains) and the DR of $(CH_3)_2COH^+$, where $(CH_3)_2COH^+$ is produced by the reactions OH + $C_3H_7^+$, H_2O + $C_3H_5^+$, and C_2H_4 + H_2COH^+. The agreement between observations and simulations for CH_3COCH_3 and C_2H_5CHO is very dependent on the efficiency of the O + C_3 reaction and

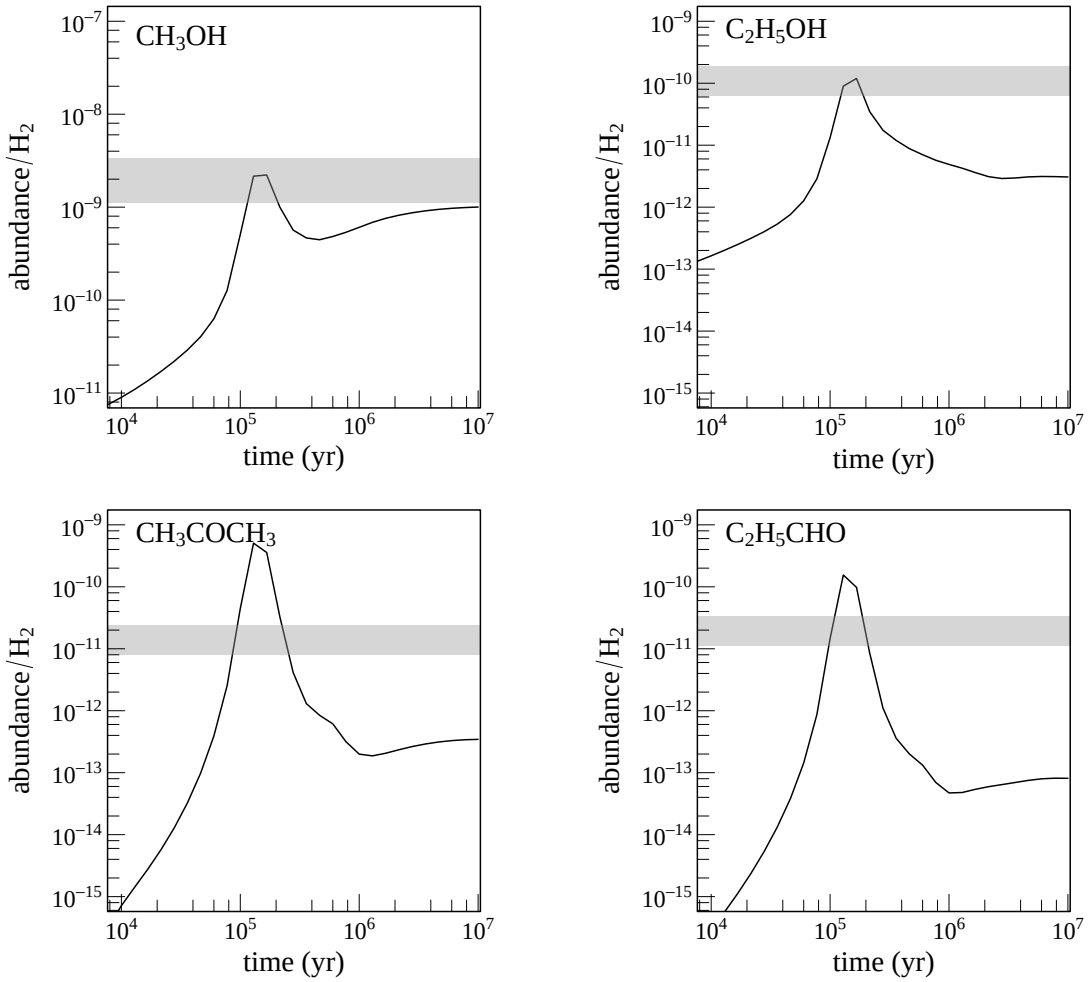

Fig. 4. Abundances of CH_3OH, C_2H_5OH, CH_3COCH_3, and C_2H_5CHO as a function of time calculated with our chemical model. The horizontal gray rectangles represent the abundances observed in TMC-1 assuming an uncertainty of a factor of three.

the efficiency of the desorption mechanisms. It is also indirectly dependent on the rate of the reactions of $C_3H_3^+$ and $C_3H_5^+$ with H_2, which are very slow at room temperature (Lin et al. 2013) but could be open at low temperature due to tunneling. These hydrogenation reactions are essential for reproducing the observations of CH_3CCH (Markwick et al. 2002) and C_3H_6 (Marcelino et al. 2007), which cannot be explained by the desorption of these species alone from the grains. It is important to emphasize the role of the O + C_3 reaction; if slow, it allows the observed O-bearing COM abundances to be reproduced but induces a very high abundance of C_3 in the gas phase, which seems incompatible with the ^{13}C fractionation of *c*-C_3H_2 (Loison et al. 2020) and the abundances of CH_3CCH and C_3H_6 around protostars (Manigand et al. 2021).

An interesting test of the ability of our chemical model to explain the chemistry of O-bearing COMs in TMC-1 is to verify if the model can account for the observed abundance of methanol. Though the production mechanisms of methanol, ethanol, acetone, and propanal are different, the chemistry on grain surfaces is significant for all these species. It is essential for CH_3OH, C_2H_5OH, and C_2H_5CHO, and important for CH_3COCH_3. For the last three molecules, grain surface chemistry plays a role because C_2H_5OH is formed from the reaction of atomic carbon with adsorbed CH_3OH, while CH_3COCH_3 and C_2H_5CHO are formed from the desorption of C_3H_x species followed by gas-phase chemistry. Similarly, the formation of methanol is essentially done on grains (more than 99%) by the successive hydrogenation of CO, with part of this methanol being injected into the gas phase via two mechanisms: desorption induced by cosmic rays (Wakelam et al. 2021) and chemical desorption (Minissale et al. 2016). It is worth noting that the formation pathway to methanol in the gas phase from the DR of protonated methanol is globally inefficient. On the one hand, the formation of $CH_3OH_2^+$ itself through either the radiative association between CH_3^+ and H_2O (Gerlich & Smith 2006) or the reaction between H_3^+ and $HCOOCH_3$ (Lawson et al. 2012) is not very efficient. On the other hand, the production of methanol is a minor channel in the DR of $CH_3OH_2^+$ with electrons (Geppert et al. 2006). The calculated abundance of CH_3OH (see Fig. 4) shows a good agreement with the value derived from observations of TMC-1 (Pratap et al. 1997; Soma et al. 2015, 2018) for a cloud age of around 2×10^5 yr, as for the other O-bearing COMs detected in this study.

5. Conclusions

We have detected, for the first time in a starless core (TMC-1), three new O-bearing COMs: ethanol, acetone, and propanal. These detections enlarge the inventory of O-bearing COMs known to be present in cold interstellar clouds, where previously other molecules of this type, such as methyl formate, dimethyl ether, propenal, and vinyl alcohol, have been found.

These molecules are present at abundance levels of 10^{-11}–10^{-10} with respect to H_2 in TMC-1. A chemical model that includes gas and dust chemistry is able to explain the formation of ethanol, acetone, and propanal in TMC-1 based on a combination of grain chemistry, nonthermal desorption, and gas-phase chemical processes.

Acknowledgements. We acknowledge funding support from Spanish Ministerio de Ciencia e Innovación through grants PID2019-106110GB-I00, PID2019-107115GB-C21, and PID2019-106235GB-I00 and from the European Research Council (ERC Grant 610256: NANOCOSMOS). J.-C.L., K.H., and V.W. acknowledge the CNRS program "Physique et Chimie du Milieu Interstellaire" (PCMI) co-funded by the Centre National d'Études Spatiales (CNES). We thank the referee for a critical reading of the article.

References

Agúndez, M., Marcelino, N., Cernicharo, J., et al. 2019, A&A, 625, A147
Agúndez, M., Marcelino, N., Tercero, B., et al. 2021, A&A, 649, A4
Bacmann, A., Taquet, V., Faure, A., et al. 2012, A&A, 541, A12
Balucani, N., Ceccarelli, C., & Taquet, V. 2015, MNRAS, 449, L16
Bermúdez, C., Bailleux, S., & Cernicharo, J. 2017, A&A, 598, A9
Blake, G. A., Sutton, E. C., Mason, C. R., & Phillips, T. G. 1987, ApJ, 315, 621
Butcher, S., & Wilson, E. B. 1964, J. Chem. Phys., 40, 1671
Cazaux, S., Tielens, A. G. G. M., Ceccarelli, C., et al. 2003, ApJ, 593, L51
Cernicharo, J., Marcelino, N., Roueff, E., et al. 2012, ApJ, 759, L43
Cernicharo, J., Marcelino, N., Agúndez, M., et al. 2020, A&A, 642, A8
Cernicharo, J., Agúndez, M., Kaiser, R. I., et al. 2021, A&A, 652, A9
Cernicharo, J., Fuentetaja, R., Agúndez, M., et al. 2022, A&A, 663, A9
Chitarra, O., Martin-Drumel, M.-A., Gans, B., et al. 2020, A&A, 644, A123
Coudert, L. H., Chitarra, O., Spaniol, J.-T., et al. 2022, J. Chem. Phys., 156, 244301
Coutens, A., Loison, J.-C., Boulanger, A., et al. 2022, A&A, 660, A6
Fossé, D., Cernicharo, J., Gerin, M., & Cox, P. 2001, ApJ, 552, 168
Garrod, R. T., Wakelam, V., & Herbst, E. 2007, A&A, 467, 1103
Garrod, R. T., Widicus Weaver, S. L., & Herbst, E. 2008, ApJ, 682, 283
Geppert, W. D., Hamberg, M., Thomas, R. D., et al. 2006, Faraday Discuss., 133, 177
Gerlich, D., & Smith, M. 2006, Phys. Scr., 73, C25
Groner, P., Albert, S., Herbst, E., et al. 2002, ApJS, 142, 145
Hamberg, M., Zhaunerchyk, V., Vigren, E., et al. 2010, A&A, 522, A90
Herbst, E. 1987, ApJ, 313, 867
Herbst, E., & Garrod, R. T. 2022, FrASS, 8, 209
Herbst, E., Giles, K., & Smith, D. 1990, ApJ, 358, 468
Hickson, K. M., Wakelam, V., & Loison, J.-C. 2016, Mol. Astrophys., 3, 1
Hickson, K. M., Loison, J.-C., & Wakelam, V. 2021, ACS Earth Space Chem., 5, 824
Hincelin, U., Wakelam, V., Hersant, F., et al. 2011, A&A, 530, A61
Hollis, J. M., Jewell, P. R., Lovas, F. J., et al. 2004, ApJ, 610, L21
Hoyermann, K., & Sievert, R. 1979, Symp. Int. Combust., 17, 517
Husain, D., & Ioannou, A. X. 1999, J. Photochem. Photobiol. A, 129, 1
Jiménez-Serra, I., Vasyunin, A. I., Caselli, P., et al. 2016, ApJ, 830, L6
Jin, M., & Garrod, R. T. 2020, ApJS, 249, 26
Lawson, P. A., Osborne, D. S., & Adams, N. G. 2012, J. Phys. Chem. A, 116, 2880
Lee, H. S., Drucker, M., & Adams, N. G. 1992, Int. J. Mass Spectrom. Ion Process., 117, 101
Lin, Z., Talbi, D., Roueff, E., et al. 2013, ApJ, 765, 80
Loison, J.-C., Wakelam, V., Gratier, P., & Hickson, K. M. 2020, MNRAS, 498, 4663
Lykke, J. M., Coutens, A., Jørgensen, J. K., et al. 2017, A&A, 597, A53
Manigand, S., Jørgensen, J. K., Calcutt, H., et al. 2020, A&A, 635, A48
Manigand, S., Coutens, A., Loison, J.-C., et al. 2021, A&A, 645, A53
Marcelino, N., Cernicharo, J., Agúndez, M., et al. 2007, ApJ, 665, L127
Markwick, A. J., Millar, T. J., & Charnley, S. B. 2002, A&A, 381, 560
Milligan, D. B., Wilson, P. F., Freeman, C. G., et al. 2002, J. Phys. Chem. A, 106, 9745
Minissale, M., Dulieu, F., Cazaux, S., & Hocuk, S. 2016, A&A, 585, A24
Müller, H. S. P., Schlöder, F., Stutzki, J., & Winnewisser, G. 2005, J. Mol. Struct., 742, 215
Müller, H. S. P., Belloche, A., Xu, L.-H., et al. 2016, A&A, 587, A92
Öberg, K. I., Bottinelli, S., Jørgensen, J. K., & van Dishoeck, E. F. 2010, ApJ, 716, 825
Pearson, J. C., Brauer, C. S., & Drouin, B. J. 2008, J. Mol. Spectr., 251, 394
Peter, R., & Dreizler, H. 1965, Z. Naturforschg., 20a, 301
Pickett, H. M., Poynter, R. L., Cohen, E. A., et al. 1998, J. Quant. Spec. Radiat. Transf., 60, 883
Pratap, P., Dickens, J. E., Snell, R. L., et al. 1997, ApJ, 486, 862
Requena-Torres, M. A., Martín-Pintado, J., Rodríguez-Franco, A., et al. 2006, A&A, 455, 971
Ruaud, M., Loison, J.-C., Hickson, K. M., et al. 2015, MNRAS, 447, 4004
Ruaud, M., Wakelam, V., & Hersant, F. 2016, MNRAS, 459, 3756
Shannon, R. J., Cossou, C., Loison, J.-C., et al. 2014, RSC Adv., 4, 26342
Shingledecker, C. N., Tennis, J., Le Gal, R., & Herbst, E. 2018, ApJ, 861, 20
Snyder, L. E., Lovas, F. J., Mehringer, D. M., et al. 2002, ApJ, 578, 245
Soma, T., Sakai, N., Watanabe, Y., & Yamamoto, S. 2015, ApJ, 802, 74
Soma, T., Sakai, N., Watanabe, Y., & Yamamoto, S. 2018, ApJ, 854, 116
Takano, M., Sasada, Y., & Satoh, T. 1968, J. Mol. Spectr., 26, 157
Tanner, S. D., Mackay, G. I., & Bohme, D. K. 1979, Can. J. Chem., 57, 2350
Taquet, V., Wirström, E. S., Charnley, S. B., et al. 2017, A&A, 607, A20
Tennis, J., Loison, J.-C., & Herbst, E. 2021, ApJ, 922, 133
Tercero, F., López-Pérez, J. A., Gallego, J. D., et al. 2021, A&A, 645, A37
Tsang, W., & Hampson, R. F. 1986, J. Phys. Chem. Ref. Data, 15, 1087
Vasyunin, A. I., & Herbst, E. 2013, ApJ, 769, 34
Wakelam, V., Dartois, E., Chabot, M., et al. 2021, A&A, 652, A63
Woon, D. E., & Herbst, E. 1996, ApJ, 465, 795
Zhao, Y., & Truhlar, D. G. 2008a, Theor. Chem. Acc., 120, 215
Zhao, Y., & Truhlar, D. G. 2008b, Acc. Chem. Res., 41, 157
Zingsheim, O., Müller, H. S. P., Lewen, F., et al. 2017, J. Mol. Spectr., 342, 125

Appendix A: Ionic formation pathways of CH_3COCH_3 and C_2H_5CHO

Herbst et al. (1990) proposed that acetone may be produced by the DR of the ion $(CH_3)_2COH^+$,

$$(CH_3)_2COH^+ + e^- \rightarrow (CH_3)_2CO + H,$$

where $(CH_3)_2COH^+$ would be formed in the reaction

$$\begin{aligned} CH_3^+ + CH_3CHO &\rightarrow (CH_3)_2COH^+ && \Delta H = -430\,\mathrm{kJ\,mol^{-1}} && 6\,\% \\ &\rightarrow C_2H_5^+ + H_2CO && \Delta H = -132\,\mathrm{kJ\,mol^{-1}} && 55\,\% \\ &\rightarrow H_2COH^+ + C_2H_4 && \Delta H = -159\,\mathrm{kJ\,mol^{-1}} && 36\,\% \\ &\rightarrow CH_3CO^+ + CH_4 && \Delta H = -333\,\mathrm{kJ\,mol^{-1}} && 3\,\%, \end{aligned}$$

for which the rate coefficient and branching ratios were measured at room temperature. The measured rate coefficient for the three-body association was used to calculate the rate coefficient of the radiative association at low temperatures using phase space theory and assuming an exit barrier to the production of bimolecular products ($C_2H_5^+ + H_2CO$, $H_2COH^+ + C_2H_4$, and $CH_3CO^+ + CH_4$).

To explore other possible $(CH_3)_2COH^+$ formation pathways, we performed various theoretical calculations on the global $(CH_3)_2COH^+$ potential energy surface using density functional theory and employing the M06-2X functional (Zhao & Trular 2008a) coupled with the aug-cc-pVTZ (AVTZ) basis set. This functional has been shown to have good accuracy for the prediction of main group thermochemistry and barrier heights (Zhao & Trular 2008b). The results of our calculations are shown in Fig. A.1.

It appears that the product channels $C_2H_5^+ + H_2CO$, $H_2COH^+ + C_2H_4$, $C_3H_5^+ + H_2O$, and $H_3O^+ + CH_3CCH$ are all barrierless, which implies a decrease in the theoretical rate coefficient of the radiative association channel with respect to the Herbst et al. (1990) value, although it opens other possible pathways for the production of $(CH_3)_2COH^+$. For the $C_2H_5^+ + H_2CO$ and $H_3O^+ + CH_3CCH$ reactions, protonation was observed to proceed in the absence of competing channels (Tanner et al. 1979; Milligan et al. 2002). The $CH_3CO^+ + CH_4$ reaction involves large barriers and does not play a role in the formation of CH_3CO or C_2H_5CHO. The two reactions, in addition to $CH_3^+ + CH_3CHO$, that can produce the protonated forms of acetone and propanal through radiative association are $H_2COH^+ + C_2H_4$ and $C_3H_5^+ + H_2O$. The calculation of these rate coefficients is beyond the scope of this article but should be done in the future. Here we used values that seem realistic (a few times $10^{-10}\,\mathrm{cm^3\,s^{-1}}$ at 10 K) as well as the maximum rate coefficient calculated by Herbst et al. (1990), $2 \times 10^{-10}\,\mathrm{cm^3\,s^{-1}}$ at 10 K, for the reaction

$$CH_3^+ + CH_3CHO \rightarrow (CH_3)_2COH^+ + h\nu.$$

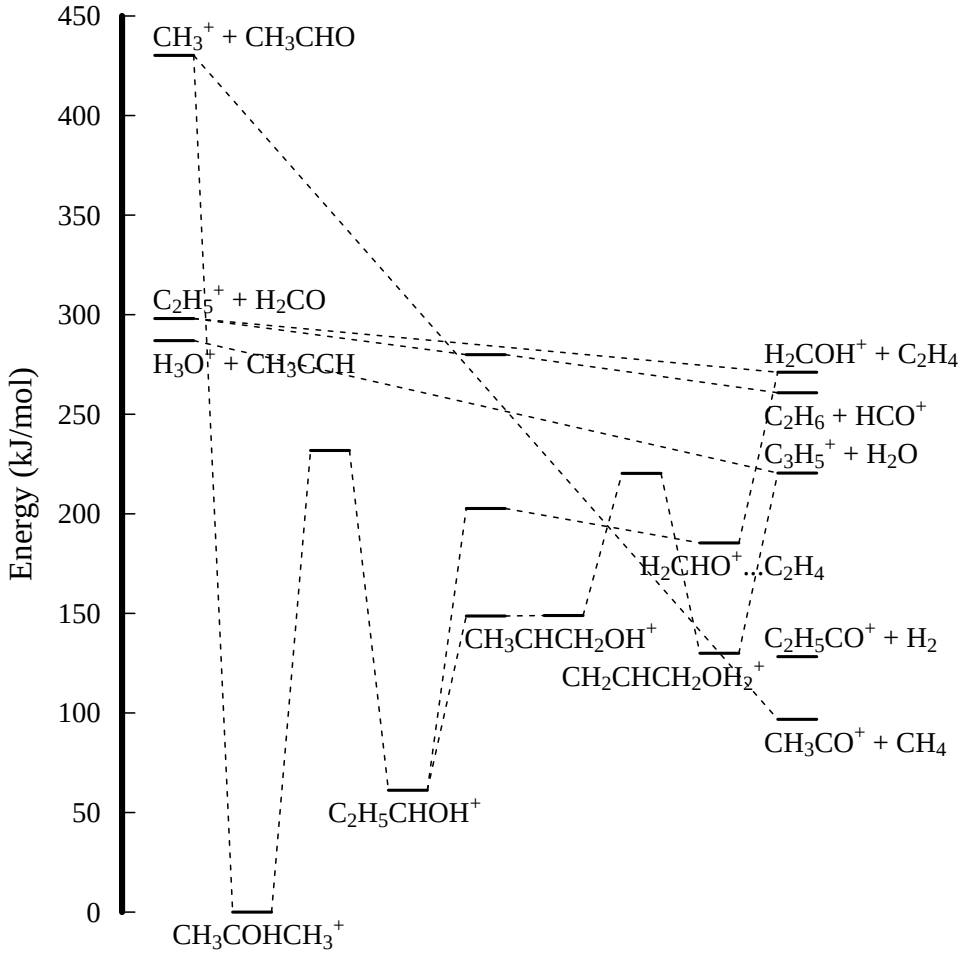

Fig. A.1. Schematic representation of the potential energy surface of $(CH_3)_2COH^+$.

However, even using these rate coefficients and considering large branching ratios (30 %) for the production of CH_3COCH_3 and C_2H_5CHO by DR of their protonated forms with electrons, the production of CH_3COCH_3 and C_2H_5CHO is largely insufficient to reproduce the observations if their protonated forms are formed only by the radiative association reactions CH_3^+ + CH_3CHO, H_2COH^+ + C_2H_4, and $C_3H_5^+$ + H_2O.

An alternative route for the production of $(CH_3)_2COH^+$ is the OH + *i*-$C_3H_7^+$ reaction:

$$\begin{aligned} OH + i-C_3H_7^+ &\rightarrow (CH_3)_2COH^+ + H \qquad \Delta H = -125\,kJ\,mol^{-1} \\ &\rightarrow CH_3CHOH^+ + CH_3 \qquad \Delta H = -99\,kJ\,mol^{-1} \\ &\rightarrow C_3H_6^+ + H_2O \qquad \Delta H = -131\,kJ\,mol^{-1} \\ &\rightarrow C_3H_5 + H_3O^+ \qquad \Delta H = -62\,kJ\,mol^{-1}. \end{aligned}$$

We studied this reaction at the M06-2X/AVTZ level and found, by relaxing the geometry at each distance, that the reaction producing the $CH_3CHOHCH_3^+$ adduct is barrierless. The evolution of this adduct can lead to different products, including $(CH_3)_2COH^+$ + H, which is the most exothermic path with a very small barrier (or none at all) in the exit channel and therefore most likely an important, if not the main, product channel.